Title

Poorer aging trajectories are associated with elevated serotonin synthesis capacity.

Journal

Molecular Psychiatry, 28(10)

Authors

Markova, Teodora

Ciampa, Claire

Parent, Jourdan

et al.

Publication Date

2023-10-01

DOI

10.1038/s41380-023-02177-x

Peer reviewed

HHS Public Access

Author manuscript

Mol Psychiatry. Author manuscript; available in PMC 2024 February 16.

Published in final edited form as:

Mol Psychiatry. 2023 October ; 28(10): 4390–4398. doi:10.1038/s41380-023-02177-x.

Poorer aging trajectories are associated with elevated serotonin synthesis capacity

Teodora Z. Markova[1], **Claire J. Ciampa**[1], **Jourdan H. Parent**[1], **Molly R. LaPoint**[2], **Mark D'Esposito**[2], **William J. Jagust**[2,3], **Anne S. Berry**[1]

[1]Brandeis University, Waltham, Massachusetts, 02453

[2]Helen Wills Neuroscience Institute, University of California Berkeley, Berkeley, California, 94720

[3]Lawrence Berkeley National Laboratory, Berkeley, California, 94720

Abstract

The dorsal raphe nucleus (DRN) is one of the earliest targets of Alzheimer's disease-related tau pathology and is a major source of brain serotonin. We used [^{18}F]Fluoro-m-tyrosine ([^{18}F]FMT) PET imaging to measure serotonin synthesis capacity in the DRN in 111 healthy adults (18-85 years-old). Similar to reports in catecholamine systems, we found elevated serotonin synthesis capacity in older adults relative to young. To establish the structural and functional context within which serotonin synthesis capacity is elevated in aging, we examined relationships among DRN [^{18}F]FMT net tracer influx (Ki) and longitudinal changes in cortical thickness using magnetic resonance imaging, longitudinal changes in self-reported depression symptoms, and AD-related tau and β-amyloid (Aβ) pathology using cross-sectional [^{18}F]Flortaucipir and [^{11}C]Pittsburgh compound-B PET respectively. Together, our findings point to elevated DRN [^{18}F]FMT Ki as a marker of poorer aging trajectories. Older adults with highest serotonin synthesis capacity showed greatest temporal lobe cortical atrophy. Cortical atrophy was associated with increasing depression symptoms over time, and these effects appeared to be strongest in individuals with highest serotonin synthesis capacity. We did not find direct relationships between serotonin synthesis capacity and AD-related pathology. Exploratory analyses revealed nuanced effects of sex within the older adult group. Older adult females showed the highest DRN synthesis capacity and exhibited the strongest relationships between entorhinal cortex tau pathology and increasing depression symptoms. Together these findings reveal PET measurement of the serotonin system to be a promising marker of aging trajectories relevant to both AD and affective changes in older age.

Corresponding Author: Teodora Markova, 415 South Street MS062, Waltham MA 02453, teodoramarkova@brandeis.edu, Phone: (781) 736 3210.

AUTHOR CONTRIBUTIONS: ASB, WJJ, MD: Conceptualization, Methodology, Validation, Resources, Supervision. **ASB, WJJ:** Investigation, Data Curation, and Project Administration. **ASB, TM, CJC, JHP, MRL:** Formal Analysis. **ASB and TM**: Writing – Original Draft. **ASB, TM,WJJ, MD, CJC, JHP, MRL:** Writing – Review and Editing. **TM:** Visualization. **ASB, WJJ, MD:** Funding Acquisition

CONFLICTS OF INTEREST

Dr. Jagust has served as a consultant for Biogen and Bioclinica and holds equity interest in Optoceutics. There are no other financial disclosures.

INTRODUCTION

In the study of Alzheimer's disease (AD), there has been a shift towards defining the very earliest changes in brain structure, function, and pathology burden, which may forecast disease trajectories. These efforts have recently focused on brainstem nuclei, including the monoamineproducing locus coeruleus and raphe complex, where abnormal tau pathology is present in middle age (1-5) and appears to precede tau deposition in the entorhinal cortex (6,7). While recent advances in magnetic resonance imaging (MRI) approaches allow for visualization of the "blue spot" (i.e. locus coeruleus), our understanding of the raphe nuclei is relatively stunted given the lack of appropriate *in vivo* neuroimaging tools. We begin to address this gap using positron emission tomography (PET) imaging to measure serotonin synthesis capacity within the raphe nuclei using the PET tracer [^{18}]Fluoro-m-tyrosine (FMT).

While the dorsal raphe nucleus (DRN) shows tau accumulation early in life, the structure appears to be quite resilient. Pathogenic changes in the DRN associated with tau burden, such as substantial cell death and shrinkage, occur later in the disease progression, once interconnected areas have also been affected (8). Though the DRN eventually shows cell loss in later AD stages (9-11), levels of the serotonin synthesis enzyme tryptophan hydroxylase do not differ from healthy controls (12), suggesting possible compensatory upregulation. Consistent with a compensation account, experimental lesioning of the raphe nuclei results in increases in forebrain tryptophan hydroxylase availability that is inversely proportional to the amount of tissue damage (13). While it is unclear to what extent upregulation of synthesis enzymes successfully preserves raphe functional integrity, these findings point to measures of raphe-serotonin synthesis as a fruitful target for investigating individual differences in aging trajectories.

The serotonin-producing raphe nuclei are a compelling focus for early detection of AD processes given associations between the serotonin system and depression, a well-known risk factor for AD (14-16). Longitudinal studies of aging suggest conversion to mild cognitive impairment can be predicted from the baseline number of depression symptoms in a dosedependent manner (17). AD processes may also exacerbate depression symptoms (18), suggesting considerable interaction between AD neuropathologic and psychopathologic processes. In contrast, healthy aging appears to be accompanied by improved emotional regulation (19) and relatively stable measures of depression (20,21). While it is unknown to what extent the raphe nuclei are implicated in mechanisms linking depression and AD, these findings point to the potential utility of tracking affective health in studies focused on the early pathogenesis of AD.

This study aimed to establish the effect of older age on serotonin synthesis capacity as measured by [^{18}F]FMT PET. To preview our results, we found higher DRN [^{18}F]FMT net tracer influx (Ki) in older adults relative to young adults. We next characterized whether higher raphe [^{18}F]FMT Ki reflected positive or negative aging trajectories by examining relationships with longitudinal change in cortical thickness, cross-sectional tau and β-amyloid (Aβ) pathology, and longitudinal change in depression symptoms in a sample of non-depressed, cognitively normal adults.

MATERIALS AND METHODS

Study design and participants

Forty-nine cognitively normal older adults are included in the current analyses and were part of the Berkeley Aging Cohort Study (mean age = 77.10, standard deviation (SD) = 5.98, range = 62-85, 29 female). Older adults were required to have undergone both [^{18}F]FMT PET scanning and [^{11}C]Pittsburgh compound-B ([^{11}C]PiB) PET scanning. A subset underwent longitudinal structural MRI (n=38), longitudinal neuropsychological testing (n=45), and cross-sectional [^{18}F]Flortaucipir PET scanning (n=43). Temporal relationships among all measures collected in older adults are illustrated in Figure 1A. Inclusion criteria for the [^{18}F]FMT scan included a Geriatric Depression Scale (GDS) score of 10 or less and a Mini-Mental State Exam score of at least 25 (Table 1). Participants had no diagnosed psychological or neurological disorders, were not taking medication to treat depression, and had no neuroimaging contraindications. Medication information was collected at each neuroimaging and neuropsychological timepoint. There was no history of selective serotonin reuptake inhibitor use cross-sectionally or longitudinally. Supplementary Table 1 lists all prescribed medications at the time of the [^{18}F]FMT scan.

To test age-group differences in serotonin synthesis capacity, 62 younger adults underwent [^{18}F]FMT PET scanning (mean age = 22.08, SD = 3.25, range = 18-32, 35 female). Young adults were recruited via advertisements at UC Berkeley. Participants did not have a history of neurological, psychological, or psychiatric disorders, and did not take medication that affects cognition, including selective serotonin reuptake inhibitors.

We report novel analyses focused on the DRN which capitalize on existing data in individuals who underwent [^{18}F]FMT PET. Power analyses (G*Power; 22) indicated sensitivity to detect medium effects 80% of the time using an alpha of .05 for between-group analyses (n = 111; Cohen's F = .27), and for within-group analyses (n = 49; f^2 = .17). We have previously reported large between-group [^{18}F]FMT PET effects (23,24), and small to large within-group effects (24-27). We acknowledge that the relatively low sample size limits our ability to detect small interaction effects and report all confidence intervals and effect sizes for transparency. The study was approved by the institutional review boards at the University of California, Berkeley, and the Lawrence Berkeley National Laboratory (LBNL). Participants gave written consent.

Cross-sectional 3T structural MRI acquisition and processing

All young and older participants underwent 3T structural scanning during a research appointment that coincided with [^{18}F]FMT PET imaging. These 3T structural scans were used for analyses of PET data. Whole-brain T1-weighted volumetric magnetization prepared rapid gradient echo image (MPRAGE) scans were collected on a 3T TIM/Trio scanner (Siemens Medical Systems; software version B17A) with a 32-channel head coil (voxel size = 1 x 1 x 1 mm^3; TR = 2300ms; matrix = 256 x 240 x 160; FPV = 256 x 240 x 160 mm^3; sagittal plan; 160 slices; 5 min acquisition time) for all older adults and 15 young adults.

Forty-seven young adults were scanned using a 12-channel head coil and T1-weighted MPRAGE scan (TR=2,300 ms; TE=2.98 ms; matrix = 240 x 256; FOV=256; sagittal plane;

voxel size = 1x1x1 mm, 160 slices). The scans were processed and segmented on FreeSurfer version 5.3 (https://surfer.nmr.mgh.harvard.edu/) and structural templates were created in Montreal Neurological Institute (MNI) 152 space using Statistical Parametric Mapping 12 (SPM12 https://www.fil.ion.ucl.ac.uk/spm/) DARTEL software.

[^{18}F]FMT PET acquisition and processing

Participants were injected with 2.5 mCi of [^{18}F]FMT synthesized at the LBNL (28). Participants ingested 2.5 mg/kg of carbidopa ~1 h before scanning to minimize the peripheral decarboxylation of [^{18}F]FMT (29-32). [^{18}F]FMT is an irreversible tracer that is a substrate for aromatic amino acid decarboxylase (AADC), the final enzyme in the synthesis reaction of serotonin from tryptophan. AADC is also involved in the synthesis of catecholamines, therefore its neurochemical specificity is dependent on the imaged brain region. We have previously reported analyses focused on [^{18}F]FMT measures within the striatum and locus coeruleus (24-26). Scanning was performed using a Siemens Biograph Truepoint 6 PET/CT scanner. We collected dynamic acquisition frames in 3D mode over 90 minutes (25 frames total, split into first 5x1 min, then 3x2 min, then 3x3 min, finally 14x5 min). Reconstructions used an ordered subset expectation maximization algorithm, taking into account scatter correction, weighted attenuation, and smoothing using a 4mm full-width and half-maximum (FWHM) Gaussian smoothing kernel. To correct for between-frame motion, we realigned to the middle frame and co-registered to each individual 3T T1-weighted scan using SPM12.

Patlak plotting was used for graphical analysis of irreversible tracer binding (30) with the primary visual cortex as the reference region, as tracer uptake in the region is low (34). Ki maps were generated from frames corresponding to 25 and 90 minutes (35,36), which represent the amount of tracer accumulated in the brain relative to the reference region. Ki can be expressed as $Ki = k_2k_3/(k_2+k_3)$, where k_2 is the rate constant for the return of free [^{18}F]FMT from the brain back to plasma and k_3 is the rate constant for the trapping of brain [^{18}F]FMT by AADC. These images are comparable to Ki images obtained using a blood input function but are scaled to the volume of tracer distribution in the reference region.

We used a DRN region of interest (ROI) as defined by Doppler and colleagues and previously used in PET imaging (37). This DRN ROI was defined based on anatomical guidelines derived from postmortem immunohistochemistry and Nissl-staining (38). Accurate coregistration to MNI space DARTEL structural templates (nearest-neighbor interpolation) was confirmed in Mango (https://www.nitrc.org/projects/mango/). The ROI was resliced to match [^{18}F]FMT Ki map voxel dimensions. While this report focuses on the DRN, we recognize the locus coeruleus is of potential interest to readers as it is also a site of early tau pathology. For completeness, we report analyses in the Supplementary Information for [^{18}F]FMT Ki measured within a locus coeruleus ROI (26).

Longitudinal 1.5T structural data acquisition and processing

1.5T T1-weighted MPRAGE scans were used for analyses of longitudinal changes in cortical thickness. Thirty-eight older participants had at least two 1.5 T1-weighted scans (mean total scans = 3.26; SD = 1.20; range = 2-6). There were not sufficient 3T data with

which to pursue longitudinal analyses. MPRAGE scans were collected on a 1.5T Magnetom Avanto System (Siemens Medical Systems) with a 12-channel head coil (TR = 2110 ms; TE = 3.58 ms; FA = 15°; matrix = 256 x 256; FOV = 256; sagittal plane; voxel size = 1 x 1 x 1 mm; 160 slices).

Structural scans were processed with FreeSurfer version 5.3. A vertex-based surface processing algorithm quantified the distance from the white matter to the closest point on the pial surface at all vertices of the cortex (39). We used FreeSurfer's longitudinal pipeline to create an unbiased within-subject template from all time points (40) using robust, inverse consistent registration (41) The template was used to increase reliability and power during longitudinal processing steps, which included motion correction, atlas registration, skull stripping, and parcellations (42). Vertex-wise statistical surface maps were created using a general linear model (GLM) framework in FreeSurfer's graphical user interface, QDEC. Before using the GLM, each participant's data were smoothed (10 mm FWHM Gaussian kernel).

Annual rate of cortical thickness change (mm/year) was calculated for each participant and either [^{18}F]FMT Ki or depression symptom slopes were used as a regressor. Vertex-wise analyses include a Monte Carlo correction for multiple comparisons ($p < .05$). Due to the heterogeneity of time differences between sessions (Figure 1A), we adjusted for between-session time differences. For longitudinal depression symptom and MRI measures, average time differences relative to the [^{18}F]FMT PET scan (including negative and positive values as pre- and post-scan, respectively) were calculated and included as covariates.

[^{11}C]PiB and [^{18}F]Flortaucipir PET acquisition and processing

All 49 older adults underwent [^{11}C]PiB scanning to assess Aβ status and a subset (n=43) underwent [^{18}F]Flortaucipir scanning to measure tau pathology (average time difference between [^{18}F]FMT and [^{18}F]Flortaucipir = 275.40 days, SD = 277.95 days; average time difference between [^{18}F]FMT and [^{11}C]PiB = 243.27 days, SD = 202.39 days). [^{11}C]PiB and [^{18}F]Flortaucipir scans were acquired within three years of the [^{18}F]FMT PET scan with the exception of one participant ([^{18}F]Flortaucipir scan 3.3 years after [^{18}F]FMT). Exclusion of this subject in analyses involving [^{18}F]Flortaucipir data did not change the results. Data acquisition for [^{11}C]PiB and [^{18}F]Flortaucipir scans was identical to protocols described previously (43). [^{11}C]PiB distribution volume ratio (DVR) images were generated using Logan graphical analysis of frames corresponding to 35 to 90 minutes after injection using the cerebellar gray matter as a reference region (44). Positive Aβ status was based on global cortical [^{11}C]PiB DVR of 1.065 or greater (45). Fourteen participants were [^{11}C]PiB positive.

[^{18}F]Flortaucipir standardized uptake volume ratio (SUVR) images were generated from frames corresponding to 80-100 min post-injection using the inferior cerebellar gray matter as a reference region and partial volume corrected as previously described (46). [^{18}F]Flortaucipir SUVR was measured within entorhinal cortex. Entorhinal cortex is the first cortical region to accumulate tau pathology (Braak I; 47) and is commonly the focus of [^{18}F]Flortaucipir-PET analyses in cognitively normal older adults (48,49).

Geriatric Depression Scale

Analyses of depression symptoms were done using the GDS, where longitudinal slopes characterizing the rate of change in depression symptoms over time were calculated using simple linear regression. Time (measured from the baseline session) was the independent variable and GDS scores for each session were the dependent variables.

Analytic rationale and statistical testing

The first goal of this study was to characterize the nature of age-group differences in DRN serotonin synthesis capacity (DRN [^{18}F]FMT Ki). We report age-group differences in serotonin synthesis capacity using an ANOVA with between-subjects factors of age-group and sex. Next, among older adults, we examined 1) the neural and behavioral correlates of higher serotonin synthesis capacity (longitudinal cortical thickness change, Aβ and tau pathology, longitudinal change in depression symptoms) 2) the role of higher serotonin synthesis capacity in resilience. We tested resilience models given previous evidence suggesting that neuromodulator systems allow older adults to “cope” (50) with cortical atrophy and pathology and are associated with the maintenance of better-than-expected cognitive trajectories (24,26). Specifically, we tested the role of serotonin synthesis capacity in moderating relationships between atrophy/pathology and longitudinal change in depression symptoms (e.g. longitudinal change in depression ~ serotonin synthesis capacity + longitudinal change in cortical thickness + serotonin synthesis capacity* longitudinal change in cortical thickness). Such interaction analyses are consistent with current frameworks for testing resilience (51).

We report direct associations among DRN serotonin synthesis capacity, longitudinal cortical thickness change, Aβ and tau pathology, and longitudinal change in depression symptoms using Pearson correlations (using IBM SPSS version 28). Secondary exploratory analyses probed effects of sex (and interactions with sex) and are corrected for multiple comparisons (False discovery rate; FDR). Moderation analyses were done using PROCESS macro, version 4.0 (52), where all variables that defined the products were mean centered. Conditional effects reported are based on moderating variable values at 1 SD above the mean, at the mean, and at 1 SD below the mean. Two subjects were excluded from analyses involving longitudinal data due to a depression symptom slope more than 3 standard deviations below the mean, and a change in cortical thickness more than 3 standard deviations above the mean. All 95% confidence intervals (CI) reflect corresponding effects of interest. Voxel-wise t-tests were done in SPM12, and subsequent results were visualized using Mango version 4.1. Given potential concerns surrounding heteroscedasticity and skewed distributions of pathology data in cognitively normal older adult populations, we replicate all primary regression analyses using bootstrapped robust regressions with the ‘robustbase’ package in R (1000 samples; 53). Robust regression statistics are reported in the Supplementary Information and replicate all significant results reported in the main manuscript. All other statistical analyses were performed using IBM SPSS version 28. Meta-data are available (https://osf.io/zbn4k/?view_only=41c30da487d845df8940a52d5df20b7f).

RESULTS

Elevated raphe [^{18}F]FMT Ki in older adults

We examined effects of age-group and sex on [^{18}F]FMT Ki measures of serotonin synthesis capacity within the DRN. An ANOVA revealed higher [^{18}F]FMT Ki in older relative to young adults ($F(1,107) = 43.48$, $p < .001$, mean difference = 0.003, 95% unstandardized CI [0.002, 0.004], $\eta_p^2 = 0.29$, Figure 1B). For visualization purposes, we display the whole-brain voxel-wise contrast demonstrating the overlap between significant age-group differences in [^{18}F]FMT Ki and the DRN ROI (Figure 1C).

There was no main effect of sex ($F(1,107) = 0.98$, $p = .326$, mean difference = 4.33E-4, 95% unstandardized CI [−0.001, 5.76E-4], $\eta_p^2 = 0.009$), but an age * sex interaction ($F(1,107) = 4.28$, $p = .041$, $\eta_p^2 = 0.04$). Post hoc t-tests revealed higher [^{18}F]FMT Ki in older adult females relative to older adult males in the DRN ($t(47) = 2.16$, $p = .036$, mean difference = 0.001, 95% unstandardized CI [0.0001, 0.0028], $d = 0.63$). No such sex-related differences were observed in the younger population ($t(60) = 0.78$, $p = .436$, mean difference = −0.001, 95% unstandardized CI [−0.0018, 0.0008], $d = 0.20$, Supplementary Figure 1).

Cortical atrophy is associated with increased [^{18}F]FMT Ki

We aimed to determine to what extent higher DRN [^{18}F]FMT Ki in aging is associated with positive or negative aging trajectories by assessing relationships between DRN [^{18}F]FMT Ki and longitudinal changes in cortical thickness. Vertex-wise regression analyses on the longitudinal structural data revealed a significant negative relationship between cortical thickness change (mm/year) and DRN [^{18}F]FMT Ki in the banks of the superior temporal sulcus, where higher synthesis capacity was associated with greater cortical atrophy (Figure 2A). This relationship survived Monte Carlo correction for multiple comparisons, as well as adjustments for age and sex and adjustments for the average time differences between the [^{18}F]FMT scan and the MRI scans for each participant (Supplementary Figure 2A, 2B). There were no positive relationships between cortical thickness change and DRN [^{18}F]FMT Ki.

Aβ, tau and [^{18}F]FMT Ki

We examined direct relationships between DRN [^{18}F]FMT Ki and Aβ and tau pathology as measured cross-sectionally with [^{11}C]PiB PET and [^{18}F]Flortaucipir PET, respectively. A twosample t-test found no significant difference in DRN [^{18}F]FMT Ki between [^{11}C]PiB negative and [^{11}C]PiB positive individuals ($t(47) = 1.74$, $p = .089$, mean difference = −0.001, 95% unstandardized CI [−0.0028, 0.0002], $d = 0.55$; Table 1). Exploratory analyses found no [^{11}C]PiB*sex interaction ($t(45) = 1.29$, $p = .203$, FDR-corrected $p = .203$, $b = 0.002$, 95% unstandardized CI [−0.001, 0.005]).

Analyses of entorhinal cortex [^{18}F]Flortaucipir SUVR found no relationship with DRN [^{18}F]FMT Ki ($r = .14$ [−0.16, 0.43], $p = .358$). Exploratory analyses found no [^{18}F]Flortaucipir*sex interaction ($t(39) = -1.20$, $p = .237$, FDR-corrected $p = .347$, $b = -0.004$, 95% unstandardized CI [−0.010, 0.003]).

[^{18}F]FMT Ki moderates the relationship between cortical atrophy and increasing depression symptoms

Next, we tested the direct association between longitudinal change in depression symptoms and DRN [^{18}F]FMT Ki, which was not significant (r = .28 [−0.02, 0.53], p = .064). While we did not find a significant direct relationship between DRN [^{18}F]FMT Ki and changes in depression symptoms, we tested a possible moderating effect of DRN [^{18}F]FMT Ki on associations between atrophy and longitudinal change in depression symptoms. We pursued this analysis to test the hypothesis that elevated serotonin synthesis capacity in aging is associated with better-thanexpected affective trajectories given one's cortical atrophy. Moderation analyses used the following model: longitudinal change in depression ~ serotonin synthesis capacity + longitudinal change in cortical thickness + serotonin synthesis capacity*longitudinal change in cortical thickness). We measured longitudinal change in cortical thickness within regions that were significantly related to both DRN [^{18}F]FMT Ki (Figure 2A) and longitudinal change in depression symptoms (Figure 2B; Supplementary Figure 2C): the left banks of the superior temporal sulcus (Figure 3A). A moderation analysis with depression symptom slope as the dependent variable identified a significant interaction between change in cortical thickness and DRN [^{18}F]FMT Ki (t(32) = −2.06, p = .048, b = −3101.91, 95% unstandardized CI [−6172.88, −30.94]; Table 2A).

Contrary to our hypotheses, higher DRN [^{18}F]FMT Ki appeared to exacerbate (rather than remediate) relationships between worsening depression symptoms and temporal lobe cortical thickness changes. Decreasing cortical thickness was associated with increasing depression symptoms over time in individuals with high DRN [^{18}F]FMT Ki (t(32) = −2.52, p = .017, b = −8.98, 95% unstandardized CI [−16.26, −1.70]; Figure 3B). Lower levels of DRN [^{18}F]FMT Ki were associated with better-than-expected depression trajectories given an individual's cortical thickness change. Analyses using the Johnson-Neyman technique (52), which determines the values of DRN [^{18}F]FMT Ki at which change in cortical thickness has a significant influence on depression symptoms, revealed that this negative relationship was significant for the top 22.2% of individuals with highest DRN [^{18}F]FMT Ki, starting at 0.0199 Ki. Adjusting for age, sex, and [^{11}C]PiB status, as well as adjusting for the average time difference between the [^{18}F]FMT PET scan, MRI scans, and depression questionnaires does not change these results (Supplementary Table 2).

Exploratory regression analyses testing interactions with sex in predicting changes in depression symptoms were null (sex * DRN [^{18}F]FMT t(40) = −0.78, p = .440, FDR-corrected p = .440, b = −67.59, 95% unstandardized CI [−242.74, 107.57]; sex * cortical thickness change t(33) = 0.36, p = .722, FDR-corrected p = .722, b = 2.97, 95% unstandardized CI [−13.90, 19.84]).

Entorhinal cortex tau pathology and change in depression symptoms

Finally, we tested direct and interactive associations between longitudinal change in depression symptoms and pathology. Change in depression symptoms did not differ based on [^{11}C]PiB status (t(42) = 0.29, p = .78, mean difference = 0.06, 95% unstandardized CI [−0.35, 0.47], d = 0.10), and was not correlated with entorhinal cortex [^{18}F]Flortaucipir SUVR (r = .23, [−0.09, 0.51], p = .159). Exploratory analyses probing interactions between

pathology and sex in predicting change in depression symptoms revealed a significant sex * entorhinal cortex [^{18}F]Flortaucipir SUVR interaction (t(35) = −2.93, p = .006, FDR-corrected p = .018, b = −2.10, 95% unstandardized CI [−3.55, −0.64]) such that females showed a positive relationship between increasing depression symptoms and higher entorhinal cortex [^{18}F]Flortaucipir SUVR (t(35) = 3.16, p = .003, b = 1.41, 95% unstandardized CI [0.51, 2.32]), which was not apparent in males (t(35) = −1.22, p = .23, b = −0.69, 95% unstandardized CI [−1.82, 0.45], Figure 3C). There was no interaction between sex and [^{11}C]PiB predicting change in depression symptoms (t(40) = −0.56, p = .576, FDR-corrected p = .864, b = −0.22, 95% unstandardized CI [−1.02, 0.57]).

We pursued moderation analyses to test the hypothesis that elevated serotonin synthesis capacity is associated with better-than-expected affective trajectories given one's tau pathology. We tested the following model: longitudinal change in depression ~ serotonin synthesis capacity + entorhinal cortex [^{18}F]Flortaucipir SUVR + serotonin synthesis capacity*entorhinal cortex [^{18}F]Flortaucipir SUVR. Moderation analyses demonstrated that levels of DRN [^{18}F]FMT Ki did significantly impact the relationship between increasing depression and entorhinal cortex [^{18}F]Flortaucipir SUVR (t(35) = 3.23, p = .003, b = 501.64, 95% unstandardized CI [186.16, 817.12], Table 2B). Contrary to our hypothesis, higher DRN [^{18}F]FMT Ki was associated with strongest relationships between higher entorhinal cortex [^{18}F]Flortaucipir SUVR and worsening depression symptoms (t(35) = 3.07, p = .004, b = 1.39, 95% unstandardized CI [0.47, 2.31], Figure 3D). Johnson-Neyman analyses revealed that this relationship was significant for the top 33.3% of individuals with the highest levels of DRN [^{18}F]FMT Ki, starting at 0.0195 Ki. The pattern of these effects was consistent with what we observed for moderation analyses involving longitudinal change in cortical thickness. Adjusting for age, sex, and [^{11}C]PiB status, as well as adjusting for the average time between the [^{18}F]FMT scan, [^{18}F]Flortaucipir scan, and depression questionnaires does not change these results (Supplementary Table 3).

DISCUSSION

This study establishes, for the first time, elevated serotonin synthesis capacity as a marker of poorer aging trajectories. In older participants, elevated DRN serotonin synthesis capacity was observed in the context of greater temporal lobe cortical atrophy. Moderation analyses did not support a role of higher synthesis capacity in successfully maintaining affective function despite cortical atrophy. Instead, relationships between greater cortical atrophy and worsening depression symptoms were strongest in individuals with elevated serotonin synthesis capacity. We found older adult females showed elevated serotonin synthesis capacity relative to males. Females with higher entorhinal tau pathology also showed worsening depression symptoms, an effect that was not seen in males. Together, these findings link age-related alterations in raphe neurochemical function and tau pathology with longitudinal changes in self-reported affect, with implications for the study of sex differences in AD vulnerability.

Using [^{18}F]FMT PET, we found elevated serotonin synthesis capacity in older adults relative to young. The direction of these findings is opposite to what one would expect if results were driven by age-related partial volume effects. The capacity for neuromodulator

systems to upregulate synthesis in the face of experimentally-induced or age and disease-related insults has been demonstrated for the serotonin (13,54), dopamine (24,55,56), norepinephrine (57-60), and acetylcholine (61,62) neuromodulator systems. Previous PET studies of serotonin synthesis capacity using α-[^{11}C]methyl-L-tryptophan, a substrate for tryptophan hydroxylase, have not reported signal in the raphe. In cortical regions, non-significant correlations with chronological age were flat or positive-going from 20-80 years old (63). The authors interpreted this pattern to reflect upregulation of synthesis or reduced vulnerability of synthesis pathways in aging.

[^{18}F]FMT uptake within serotonin-producing nuclei has been described in non-human primates (34). To our knowledge, this is the first report focusing on [^{18}F]FMT Ki within the raphe nuclei in humans. Validation studies and studies in non-human primates find [^{18}F]FMT has true irreversible uptake into monoamine-synthesizing neurons, where it is decarboxylated by AADC and remains trapped within the intracellular space (64-67) with strong correlations between [^{18}F]FMT Ki and AADC activity (68). Suggesting AADC is a very stable protein, it has slow turn-over rates of over 3.5 days (69). That said, it is not clear whether higher [^{18}F]FMT Ki in aging reflects higher density of AADC or greater activity of AADC, perhaps via greater rates of phosphorylation by protein kinases A or G (70,71). AADC activity can be augmented in response to receptor antagonism (e.g. 5-HT1A; 5-HT2A) as well as by alterations in hormones and trophic factors (72-74). Short-term AADC regulation has been mostly attributed to kinase activity, whereas longer-term regulation has been attributed to changes in mRNA transcript levels and thus presumably protein levels (75). Additional biological data are needed to define the mechanisms contributing to higher [^{18}F]FMT Ki in aging in addition to complementary studies defining how [^{18}F]FMT Ki measures functionally relate to serotonin availability and receptor density across the lifespan.

While apparent upregulation is often interpreted to be compensatory, whether this upregulation successfully rescues function may be highly system and disease dependent. In the case of the serotonin system in aging, it may be that the preservation of “youth-like” levels of synthesis are a sign of healthy aging while elevation is a sign of pathological trajectories that exacerbate effects of atrophy and tau pathology on depression symptoms. This is in contrast to our recent findings identifying elevated striatal dopamine synthesis capacity as a successful cognitive reserve mechanism, reducing the negative associations between atrophy and executive function decline (24). Further, elevated locus coeruleus catecholamine synthesis capacity has also been identified as a candidate cognitive reserve mechanism, reducing the negative association between higher temporal lobe tau pathology and lower memory performance (26). Longitudinal [^{18}F]FMT studies will be critical for tracking the temporal pattern of apparent increases in serotonin synthesis to define windows for which upregulation may be functionally beneficial.

Though MRI methods for assessing the raphe are limited, PET imaging has been recognized as a promising tool for localizing the raphe nuclei (15,76) and tracking the progression of neurodegenerative disorders such as Parkinson’s disease (37,58). There has been relatively little *in vivo* imaging of age and AD-related changes in the serotonin system. Existing studies have largely reported lower or unchanged serotonin receptor density (5-HT1A,

5-HT1B) and transporter density in aging and AD (15,77). In aging, there is some evidence for upregulation of autoreceptors in the raphe (77,78). There is a need for programmatic research investigating the progression of both presynaptic and postsynaptic alterations in the raphe nuclei and connected structures. Bolstering our understanding of the DRN in aging will be essential for investigating the converging and diverging roles of monoamine and catecholamine-producing nuclei in AD pathologic processes (7,25,79,80), which is particularly important given their mutual modulation of affective function and relevance to psychopathology (25,81,82).

There is tremendous interest in understanding the neurobiological basis of female's vulnerability to AD and mood disorders. The extent to which there is a common biological substrate is unknown. Previous research has demonstrated sex differences in various measures of the serotonin system including synthesis capacity (83-85) and receptor density (86). We found significantly higher DRN [^{18}F]FMT Ki in older adult females relative to males—a sex difference which was absent in youth. It is not clear why sex differences might arise in older age. Longitudinal studies are needed to replicate and extend this finding within-subject and may probe possible effects of menopause. Future research is needed to test whether the serotonin system is more reactive to insult in females than it is in males, perhaps by responding to reductions in structural integrity or losses in receptor density with outsized enzymatic upregulation.

This study has limitations. There were long temporal delays between PET scans and variations in the span of available longitudinal measures. Further, longitudinal behavioral and neuroimaging studies are limited by possible selection bias—meaning those individuals who maintain participation in the study are exceptional and not wholly representative of the broader population. The relatively small sample limited our ability to rigorously test moderation effects and possible effects of sex and Aβ status on our results. For example, differences in DRN serotonin synthesis capacity between Aβ positive and negative individuals did not reach statistical significance, but should be the focus of future research given links between serotonin signaling and Aβ metabolism and deposition (87-89). A focus on Aβ positive individuals has the advantage of enriching the study sample with more individuals with higher levels of tau and promises to enhance the interpretability of our findings in the context of AD, as both entorhinal cortex tau pathology and cortical atrophy arise in aging independent of AD pathological processes. The raphe nuclei receive input from catecholamine-producing nuclei. Thus, it is possible the [^{18}F]FMT signal we are measuring also has contributions from AADC activity in the presynaptic terminals of these catecholamine projections. As this was not a clinically depressed sample, it is not known whether these results will translate to individuals with higher levels of depression symptoms. Future longitudinal studies including longitudinal [^{18}F]FMT are needed.

Together, these findings reveal [^{18}F]FMT PET to be a novel marker of aging trajectories. There is an acute need to develop neuroimaging programs tracking alterations in raphe structure and function to complement research focused on the catecholaminergic locus coeruleus (90) and cholinergic basal forebrain (91). Understanding the common and distinct patterns of pathological processes in these regions promises to shed light on the neural basis of individual differences in AD clinical progression and disease manifestation.

Supplementary Material

Refer to Web version on PubMed Central for supplementary material.

ACKNOWLEDGEMENTS

This research was supported by the following grants: National Institutes of Health grant AG058748 (ASB), AG072328 (ASB), AG034570 (WJJ), AG062542 (WJJ), AG044292 (WJJ), DA034685 (MD), and Alzheimer's Association Award AARF-17-530186 (ASB). Avid Radiopharmaceuticals enabled the use of the Flortaucipir tracer but did not provide direct funding and were not involved in data analysis or interpretation. MR data were collected at the Henry H. Wheeler, Jr. Brain Imaging Center, which receives support from the National Science Foundation through their Major Research Instrumentation Program, award number BCS-0821855. We thank Michael Sommerauer for generously sharing the raphe region of interest.

REFERENCES

1. Andrés-Benito P, Fernández-Dueñas V, Carmona M, Escobar LA, Torrejón-Escribano B, Aso E, et al. Locus coeruleus at asymptomatic early and middle Braak stages of neurofibrillary tangle pathology. Neuropathol Appl Neurobiol. 2017 Aug;43(5):373–92. [PubMed: 28117912]
2. Parvizi J, Van Hoesen GW, Damasio A. The selective vulnerability of brainstem nuclei to Alzheimer's disease. Ann Neurol. 2001;49(1):53–66. [PubMed: 11198297]
3. Rüb U, Stratmann K, Heinsen H, Del Turco D, Seidel K, den Dunnen W, et al. The Brainstem Tau Cytoskeletal Pathology of Alzheimer's Disease: A Brief Historical Overview and Description of its Anatomical Distribution Pattern, Evolutional Features, Pathogenetic and Clinical Relevance. Curr Alzheimer Res. 2016 Oct 1;13(10):1178–97. [PubMed: 27264543]
4. Šimić G, Leko MB, Wray S, Harrington C, Delalle I, Jovanov-Milošević N, et al. Monoaminergic Neuropathology in Alzheimer's disease. Prog Neurobiol. 2017 Apr;151:101–38. [PubMed: 27084356]
5. Stratmann K, Heinsen H, Korf H, Del Turco D, Ghebremedhin E, Seidel K, et al. Precortical Phase of Alzheimer's Disease (AD)-Related Tau Cytoskeletal Pathology. Brain Pathol. 2015 Aug 24;26(3):371–86. [PubMed: 26193084]
6. Braak H, Thal DR, Ghebremedhin E, Del Tredici K. Stages of the Pathologic Process in Alzheimer Disease: Age Categories From 1 to 100 Years. J Neuropathol Exp Neurol. 2011 Nov 1;70(11):960–9. [PubMed: 22002422]
7. Grinberg LT, Rüb U, Ferretti REL, Nitrini R, Farfel JM, Polichiso L, et al. The dorsal raphe nucleus shows phospho-tau neurofibrillary changes before the transentorhinal region in Alzheimer's disease. A precocious onset? Neuropathol Appl Neurobiol. 2009 Aug;35(4):406–16. [PubMed: 19508444]
8. Ehrenberg AJ, Nguy AK, Theofilas P, Dunlop S, Suemoto CK, Di Lorenzo Alho AT, et al. Quantifying the accretion of hyperphosphorylated tau in the locus coeruleus and dorsal raphe nucleus: the pathological building blocks of early Alzheimer's disease. Neuropathol Appl Neurobiol. 2017 Aug;43(5):393–408. [PubMed: 28117917]
9. Aletrino MA, Vogels OJM, Van Domburg PHMF, Ten Donkelaar HJ. Cell loss in the nucleus raphes dorsalis in alzheimer's disease. Neurobiol Aging. 1992 Jul;13(4):461–8. [PubMed: 1508296]
10. Gottfries CG, Bartfai T, Carlsson A, Eckernäs S, Svennerholm L. Multiple biochemical deficits in both gray and white matter of Alzheimer brains. Prog Neuropsychopharmacol Biol Psychiatry. 1986;10(3–5):405–13. [PubMed: 3797685]
11. Palmer AM, Wilcock GK, Esiri MM, Francis PT, Bowen DM. Monoaminergic innervation of the frontal and temporal lobes in Alzheimer's disease. Brain Res. 1987 Jan 20;401(2):231–8. [PubMed: 2434191]
12. Storga D, Vrecko K, Birkmayer JGD, Reibnegger G. Monoaminergic neurotransmitters, their precursors and metabolites in brains of Alzheimer patients. Neurosci Lett. 1996 Jan 12;203(1):29–32. [PubMed: 8742039]
13. Geyer MA, Puerto A, Dawsey WJ, Knapp S, Bullard WP, Mandell AJ. Histologic and enzymatic studies of the mesolimbic and mesostriatal serotonergic pathways. Brain Res. 1976 Apr;106(2):241–56. [PubMed: 6112]

14. Diniz BS, Butters MA, Albert SM, Dew MA, Reynolds CF. Late-life depression and risk of vascular dementia and Alzheimer's disease: systematic review and meta-analysis of community-based cohort studies. Br J Psychiatry. 2013 May;202(5):329–35. [PubMed: 23637108]
15. Meltzer MDC Serotonin in Aging, Late-Life Depression, and Alzheimer's Disease: The Emerging Role of Functional Imaging. Neuropsychopharmacology. 1998 Jun;18(6):407–30. [PubMed: 9571651]
16. Ownby RL, Crocco E, Acevedo A, John V, Loewenstein D. Depression and Risk for Alzheimer Disease. Arch Gen Psychiatry. 2006 May;63(5):530–8. [PubMed: 16651510]
17. Han FF, Wang HX, Wu JJ, Yao W, Hao CF, Pei JJ. Depressive symptoms and cognitive impairment: A 10-year follow-up study from the Survey of Health, Ageing and Retirement in Europe. Eur Psychiatry. 2021 Aug 27;64(1):e55. [PubMed: 34446123]
18. Krell-Roesch J, Syrjanen JA, Rakusa M, Vemuri P, Machulda MM, Kremers WK, et al. Association of Cortical and Subcortical β-Amyloid With Standardized Measures of Depressive and Anxiety Symptoms in Adults Without Dementia. J Neuropsychiatry Clin Neurosci. 2021 Jan;33(1):64–71. [PubMed: 33086924]
19. Gurera JW, Isaacowitz DM. Emotion regulation and emotion perception in aging: A perspective on age-related differences and similarities. In: Emotion and cognition. San Diego, CA, US: Elsevier Academic Press; 2019. p. 329–51. (Progress in brain research).
20. Cotter DL, Walters SM, Fonseca C, Wolf A, Cobigo Y, Fox EC, et al. Aging and Positive Mood: Longitudinal Neurobiological and Cognitive Correlates. Am J Geriatr Psychiatry Off J Am Assoc Geriatr Psychiatry. 2020 Sep;28(9):946–56.
21. Jorm AF. Does old age reduce the risk of anxiety and depression? A review of epidemiological studies across the adult life span. Psychol Med. 2000 Jan;30(1):11–22. [PubMed: 10722172]
22. Faul F, Erdfelder E, Lang AG, Buchner A. G*Power 3: a flexible statistical power analysis program for the social, behavioral, and biomedical sciences. Behav Res Methods. 2007 May;39(2):175–91. [PubMed: 17695343]
23. Berry AS, Shah VD, Baker SL, Vogel JW, O'Neil JP, Janabi M, et al. Aging Affects Dopaminergic Neural Mechanisms of Cognitive Flexibility. J Neurosci Off J Soc Neurosci. 2016 Dec 14;36(50):12559–69.
24. Ciampa CJ, Parent JH, Lapoint MR, Swinnerton KN, Taylor MM, Tennant VR, et al. Elevated Dopamine Synthesis as a Mechanism of Cognitive Resilience in Aging. Cereb Cortex. 2022 Jun 16;32(13):2762–72. [PubMed: 34718454]
25. Parent JH, Ciampa CJ, Harrison TM, Adams JN, Zhuang K, Betts MJ, et al. Locus coeruleus catecholamines link neuroticism and vulnerability to tau pathology in aging. NeuroImage. 2022 Sep 30;119658. [PubMed: 36191755]
26. Ciampa CJ, Parent JH, Harrison TM, Fain RM, Betts MJ, Maass A, et al. Associations among locus coeruleus catecholamines, tau pathology, and memory in aging. Neuropsychopharmacology. 2022 Apr;47(5):1106–13. [PubMed: 35034099]
27. Berry AS, Shah VD, Jagust WJ. The Influence of Dopamine on Cognitive Flexibility Is Mediated by Functional Connectivity in Young but Not Older Adults. J Cogn Neurosci. 2018 Sep;30(9):1330–44. [PubMed: 29791298]
28. VanBrocklin HF, Blagoev M, Hoepping A, O'Neil JP, Klose M, Schubiger PA, et al. A new precursor for the preparation of 6-[18F]Fluoro-l-m-tyrosine ([18F]FMT): efficient synthesis and comparison of radiolabeling. Appl Radiat Isot. 2004 Dec 1;61(6):1289–94. [PubMed: 15388123]
29. Boyes BE, Cumming P, Martin WRW, McGeer EG. Determination of plasma [18F]-6fluorodopa during positron emission tomography: Elimination and metabolism in carbidopa treated subjects. Life Sci. 1986 Dec 8;39(23):2243–52. [PubMed: 3097437]
30. Firnau G, Sood S, Chirakal R, Nahmias C, Garnett ES. Metabolites of 6-[18F]fluoro-L-dopa in human blood. J Nucl Med Off Publ Soc Nucl Med. 1988 Mar;29(3):363–9.
31. Hoffman JM, Melega WP, Hawk TC, Grafton SC, Luxen A, Mahoney DK, et al. The effects of carbidopa administration on 6-[18F]fluoro-L-dopa kinetics in positron emission tomography. J Nucl Med Off Publ Soc Nucl Med. 1992 Aug;33(8):1472–7.

32. Melega WP, Hoffman JM, Luxen A, Nissenson CH, Phelps ME, Barrio JR. The effects of carbidopa on the metabolism of 6-[18F]fluoro-L-dopa in rats, monkeys and humans. Life Sci. 1990;47(2):149–57. [PubMed: 2117691]
33. Patlak CS, Blasberg RG. Graphical Evaluation of Blood-to-Brain Transfer Constants from Multiple-Time Uptake Data. Generalizations. J Cereb Blood Flow Metab. 1985 Dec 1;5(4):584–90. [PubMed: 4055928]
34. Brown WD, DeJesus OT, Pyzalski RW, Malischke L, Roberts AD, Shelton SE, et al. Localization of trapping of 6-[18F]fluoro-L-m-tyrosine, an aromatic L-amino acid decarboxylase tracer for PET. Synapse. 1999;34(2):111–23. [PubMed: 10502310]
35. Ito H, Ota M, Ikoma Y, Seki C, Yasuno F, Takano A, et al. Quantitative analysis of dopamine synthesis in human brain using positron emission tomography with L-[β11C]DOPA. Nucl Med Commun. 2006 Sep;27(9):723–31. [PubMed: 16894327]
36. Ito H, Shidahara M, Takano H, Takahashi H, Nozaki S, Suhara T. Mapping of central dopamine synthesis in man, using positron emission tomography with l-[β-11C]DOPA. Ann Nucl Med. 2007 Aug 1;21(6):355–60. [PubMed: 17705016]
37. Doppler CEJ, Kinnerup MB, Brune C, Farrher E, Betts M, Fedorova TD, et al. Regional locus coeruleus degeneration is uncoupled from noradrenergic terminal loss in Parkinson's disease. Brain. 2021 Oct 22;144(9):2732–44. [PubMed: 34196700]
38. Kranz GS, Hahn A, Savli M, Lanzenberger R. Challenges in the differentiation of midbrain raphe nuclei in neuroimaging research. Proc Natl Acad Sci [Internet]. 2012 Jul 17 [cited 2022 Jul 25];109(29). Available from: https://pnas.org/doi/full/10.1073/pnas.1206247109
39. Fischl B, Dale AM. Measuring the thickness of the human cerebral cortex from magnetic resonance images. Proc Natl Acad Sci. 2000 Sep 26;97(20):11050–5. [PubMed: 10984517]
40. Reuter M, Fischl B. Avoiding asymmetry-induced bias in longitudinal image processing. NeuroImage. 2011;57(1):19–21. [PubMed: 21376812]
41. Reuter M, Rosas HD, Fischl B. Highly accurate inverse consistent registration: a robust approach. NeuroImage. 2010 Dec;53(4):1181–96. [PubMed: 20637289]
42. Reuter M, Schmansky NJ, Rosas HD, Fischl B. Within-subject template estimation for unbiased longitudinal image analysis. NeuroImage. 2012 Jul 16;61(4):1402–18. [PubMed: 22430496]
43. Schöll M, Lockhart SN, Schonhaut DR, O'Neil JP, Janabi M, Ossenkoppele R, et al. PET Imaging of Tau Deposition in the Aging Human Brain. Neuron. 2016 Mar 2;89(5):971–82. [PubMed: 26938442]
44. Price JC, Klunk WE, Lopresti BJ, Lu X, Hoge JA, Ziolko SK, et al. Kinetic modeling of amyloid binding in humans using PET imaging and Pittsburgh Compound-B. J Cereb Blood Flow Metab Off J Int Soc Cereb Blood Flow Metab. 2005 Nov;25(11):1528–47.
45. Villeneuve S, Rabinovici G, Cohn-Sheehy B, Madison C, Ayakta N, Ghosh P, et al. Existing Pittsburgh Compound-B positron emission tomography thresholds are too high: statistical and pathological evaluation. Brain. 2015;138(Pt 7).
46. Baker SL, Maass A, Jagust WJ. Considerations and code for partial volume correcting [18F]AV-1451 tau PET data. Data Brief. 2017 Dec;15:648–57. [PubMed: 29124088]
47. Braak H, Braak E. Neuropathological stageing of Alzheimer-related changes. Acta Neuropathol (Berl). 1991 Sep 1;82(4):239–59. [PubMed: 1759558]
48. Maass A, Lockhart SN, Harrison TM, Bell RK, Mellinger T, Swinnerton K, et al. Entorhinal Tau Pathology, Episodic Memory Decline, and Neurodegeneration in Aging. J Neurosci. 2018 Jan 17;38(3):530–43. [PubMed: 29192126]
49. Harrison TM, Maass A, Adams JN, Du R, Baker SL, Jagust WJ. Tau deposition is associated with functional isolation of the hippocampus in aging. Nat Commun. 2019 Oct 25;10(1):4900. [PubMed: 31653847]
50. Arenaza-Urquijo EM, Vemuri P. Resistance vs resilience to Alzheimer disease. Neurology. 2018 Apr 10;90(15):695–703. [PubMed: 29592885]
51. Stern Y, Arenaza-Urquijo EM, Bartrés-Faz D, Belleville S, Cantilon M, Chetelat G, et al. Whitepaper: Defining and investigating cognitive reserve, brain reserve, and brain maintenance. Alzheimers Dement J Alzheimers Assoc. 2020 Sep;16(9):1305–11.

52. Hayes Andrew F. Introduction to Mediation, Moderation, and Conditional Process Analysis. 3rd edition. New York: The Guilford Press; 2022.
53. Maechler M, Rousseeuw P, Croux C, Todorov V, Ruckstuhl A, Salibian-Barrera M, et al. robustbase: Basic Robust Statistics. R package version 0.99–0, http://robustbase.r-forge.rproject.org/. 2023
54. Tsuiki K, Mück-Šeler D, Diksic M. Autoradiographic evaluation of the influence of hypothalamic 5,7-dihydroxytryptamine lesion on brain serotonin synthesis. Biochem Pharmacol. 1995 Mar 1;49(5):633–42. [PubMed: 7887978]
55. Dejesus OT, Endres CJ, Shelton SE, Nickles RJ, Holden JE. Noninvasive assessment of aromatic L-amino acid decarboxylase activity in aging rhesus monkey brain in vivo. Synapse. 2001;39(1):58–63. [PubMed: 11071710]
56. Eberling JL, Roberts JA, Taylor SE, VanBrocklin HF, O'Neil JP, Nordahl TE. No effect of age and estrogen on aromatic L- amino acid decarboxylase activity in rhesus monkey brain. Neurobiol Aging. 2002 May 1;23(3):479–83. [PubMed: 11959410]
57. Moore RY, Whone AL, Brooks DJ. Extrastriatal monoamine neuron function in Parkinson's disease: An 18F-dopa PET study. Neurobiol Dis. 2008 Mar 1;29(3):381–90. [PubMed: 18226536]
58. Pavese N, Rivero-Bosch M, Lewis SJ, Whone AL, Brooks DJ. Progression of monoaminergic dysfunction in Parkinson's disease: A longitudinal 18F-dopa PET study. NeuroImage. 2011 Jun 1;56(3):1463–8. [PubMed: 21396455]
59. Fritschy JM, Grzanna R. Restoration of ascending noradrenergic projections by residual locus coeruleus neurons: compensatory response to neurotoxin-induced cell death in the adult rat brain. J Comp Neurol. 1992 Jul 15;321(3):421–41. [PubMed: 1506478]
60. Acheson AL, Zigmond MJ. Short and long term changes in tyrosine hydroxylase activity in rat brain after subtotal destruction of central noradrenergic neurons. J Neurosci. 1981 May 1;1(5):493–504. [PubMed: 6125573]
61. Lapchak PA, Jenden DJ, Heft F. Compensatory elevation of acetylcholine synthesis in vivo by cholinergic neurons surviving partial lesions of the septohippocampal pathway. J Neurosci. 1991;2821–8. [PubMed: 1880551]
62. DeKosky ST, Ikonomovic MD, Styren SD, Beckett L, Wisniewski S, Bennett DA, et al. Upregulation of choline acetyltransferase activity in hippocampus and frontal cortex of elderly subjects with mild cognitive impairment. Ann Neurol. 2002 Feb;51(2):145–55. [PubMed: 11835370]
63. Rosa-Neto P, Benkelfat C, Sakai Y, Leyton M, Morais JA, Diksic M. Brain regional α[11C]methyl-L-tryptophan trapping, used as an index of 5-HT synthesis, in healthy adults: absence of an age effect. Eur J Nucl Med Mol Imaging. 2007 Aug;34(8):1254–64. [PubMed: 17318550]
64. DeJesus OT. Positron-labeled DOPA analogs to image dopamine terminals. Drug Dev Res. 2003 Jun;59(2):249–60.
65. Nahmias C, Wahl L, Chirakal R, Firnau G, Garnett ES. A probe for intracerebral aromatic amino-acid decarboxylase activity: Distribution and kinetics of [18F]6-fluoro-L-m-tyrosine in the human brain. Mov Disord. 1995;10(3):298–304. [PubMed: 7651447]
66. DeJesus OT, Endres CJ, Shelton SE, Nickles RJ, Holden JE. Evaluation of fluorinated mtyrosine analogs as PET imaging agents of dopamine nerve terminals: comparison with 6fluoroDOPA. J Nucl Med Off Publ Soc Nucl Med. 1997 Apr;38(4):630–6.
67. Brown WD, DeJesus OT, Pyzalski RW, Malischke L, Roberts AD, Shelton SE, et al. Localization of trapping of 6-[(18)F]fluoro-L-m-tyrosine, an aromatic L-amino acid decarboxylase tracer for PET. Synap N Y N. 1999 Nov;34(2):111–23.
68. Fiandaca MS, Varenika V, Eberling J, McKnight T, Bringas J, Pivirotto P, et al. Real-time MR imaging of adeno-associated viral vector delivery to the primate brain. NeuroImage. 2009 Aug 1;47:T27–35. [PubMed: 19095069]
69. DeJesus OT, Flores LG, Murali D, Converse AK, Bartlett RM, Barnhart TE, et al. Aromatic l-amino acid decarboxylase turnover in vivo in rhesus macaque striatum: A microPET study. Brain Res. 2005 Aug 23;1054(1):55–60. [PubMed: 16055094]

70. Duchemin AM, Neff NH, Hadjiconstantinou M. Aromatic l-amino acid decarboxylase phosphorylation and activation by PKGIαin vitro. J Neurochem. 2010;114(2):542–52. [PubMed: 20456015]
71. Duchemin AM, Berry MD, Neff NH, Hadjiconstantinou M. Phosphorylation and activation of brain aromatic L-amino acid decarboxylase by cyclic AMP-dependent protein kinase. J Neurochem. 2000 Aug;75(2):725–31. [PubMed: 10899948]
72. Neff NH, Wemlinger TA, Duchemin AM, Hadjiconstantinou M. Clozapine Modulates Aromatic l-Amino Acid Decarboxylase Activity in Mouse Striatum. J Pharmacol Exp Ther. 2006 May 1;317(2):480–7. [PubMed: 16415089]
73. Li XM, Juorio AV, Boulton AA. Induction of aromatic L-amino acid decarboxylase mRNA by interleukin-1 beta and prostaglandin E2 in PC12 cells. Neurochem Res. 1994 May;19(5):591–5. [PubMed: 8065515]
74. Snyder SH, Axelrod J, Wurtman RJ. Effect of Gonadal Hormones on Aromatic Amino Acid Decarboxylase in the Rat Uterus. Endocrinology. 1966 Jun 1;78(6):1135–8. [PubMed: 5296891]
75. Hadjiconstantinou M, Neff NH. Enhancing Aromatic L-amino Acid Decarboxylase Activity: Implications for L-DOPA Treatment in Parkinson's Disease. CNS Neurosci Ther. 2008;14(4):340–51. [PubMed: 19040557]
76. Beliveau V, Svarer C, Frokjaer VG, Knudsen GM, Greve DN, Fisher PM. Functional connectivity of the dorsal and median raphe nuclei at rest. NeuroImage. 2015 Aug 1;116:187–95. [PubMed: 25963733]
77. Karrer TM, McLaughlin CL, Guaglianone CP, Samanez-Larkin GR. Reduced serotonin receptors and transporters in normal aging adults: a meta-analysis of PET and SPECT imaging studies. Neurobiol Aging. 2019 Aug;80:1–10. [PubMed: 31055162]
78. Møller M, Jakobsen S, Gjedde A. Parametric and regional maps of free serotonin 5HT1A receptor sites in human brain as function of age in healthy humans. Neuropsychopharmacol Off Publ Am Coll Neuropsychopharmacol. 2007 Aug;32(8):1707–14.
79. Grinberg LT, Rueb U, Heinsen H. Brainstem: Neglected Locus in Neurodegenerative Diseases. Front Neurol [Internet]. 2011 [cited 2022 Aug 17];2. Available from: http://journal.frontiersin.org/article/10.3389/fneur.2011.00042/abstract
80. Jacobs HIL, Becker JA, Kwong K, Engels-Domínguez N, Prokopiou PC, Papp KV, et al. In vivo and neuropathology data support locus coeruleus integrity as indicator of Alzheimer's disease pathology and cognitive decline. Sci Transl Med. 2021 Sep 22;13(612):eabj2511. [PubMed: 34550726]
81. Dulawa SC, Janowsky DS. Cholinergic Regulation of Mood: From Basic and Clinical Studies to Emerging Therapeutics. Mol Psychiatry. 2019 May;24(5):694–709. [PubMed: 30120418]
82. Dunlop BW, Nemeroff CB. The Role of Dopamine in the Pathophysiology of Depression. Arch Gen Psychiatry. 2007 Mar 1;64(3):327–37. [PubMed: 17339521]
83. Frey BN, Skelin I, Sakai Y, Nishikawa M, Diksic M. Gender differences in α-[11C]MTrp brain trapping, an index of serotonin synthesis, in medication-free individuals with major depressive disorder: A positron emission tomography study. Psychiatry Res Neuroimaging. 2010 Aug;183(2):157–66.
84. Sakai Y, Nishikawa M, Leyton M, Benkelfat C, Young SN, Diksic M. Cortical trapping of α[11C]methyl-l-tryptophan, an index of serotonin synthesis, is lower in females than males. NeuroImage. 2006 Nov 15;33(3):815–24. [PubMed: 16996279]
85. Nishizawa S, Benkelfat C, Young SN, Leyton M, Mzengeza S, de Montigny C, et al. Differences between males and females in rates of serotonin synthesis in human brain. Proc Natl Acad Sci. 1997 May 13;94(10):5308–13. [PubMed: 9144233]
86. Jovanovic H, Lundberg J, Karlsson P, Cerin Å, Saijo T, Varrone A, et al. Sex differences in the serotonin 1A receptor and serotonin transporter binding in the human brain measured by PET. NeuroImage. 2008 Feb;39(3):1408–19. [PubMed: 18036835]
87. Colaianna M, Tucci P, Zotti M, Morgese MG, Schiavone S, Govoni S, et al. Soluble beta amyloid(1-42): a critical player in producing behavioural and biochemical changes evoking depressive-related state? Br J Pharmacol. 2010 Apr;159(8):1704–15. [PubMed: 20218978]

88. Sheline YI, West T, Yarasheski K, Swarm R, Jasielec MS, Fisher JR, et al. An antidepressant decreases CSF Aβ production in healthy individuals and in transgenic AD mice. Sci Transl Med. 2014 May 14;6(236):236re4.

89. Cirrito JR, Disabato BM, Restivo JL, Verges DK, Goebel WD, Sathyan A, et al. Serotonin signaling is associated with lower amyloid-β levels and plaques in transgenic mice and humans. Proc Natl Acad Sci. 2011 Sep 6;108(36):14968–73. [PubMed: 21873225]

90. Matchett BJ, Grinberg LT, Theofilas P, Murray ME. The mechanistic link between selective vulnerability of the locus coeruleus and neurodegeneration in Alzheimer's disease. Acta Neuropathol (Berl). 2021 May 1;141(5):631–50. [PubMed: 33427939]

91. Berry AS, Harrison TM. New perspectives on the basal forebrain cholinergic system in Alzheimer's disease. Neurosci Biobehav Rev. 2023 Jul;150:105192. [PubMed: 37086935]

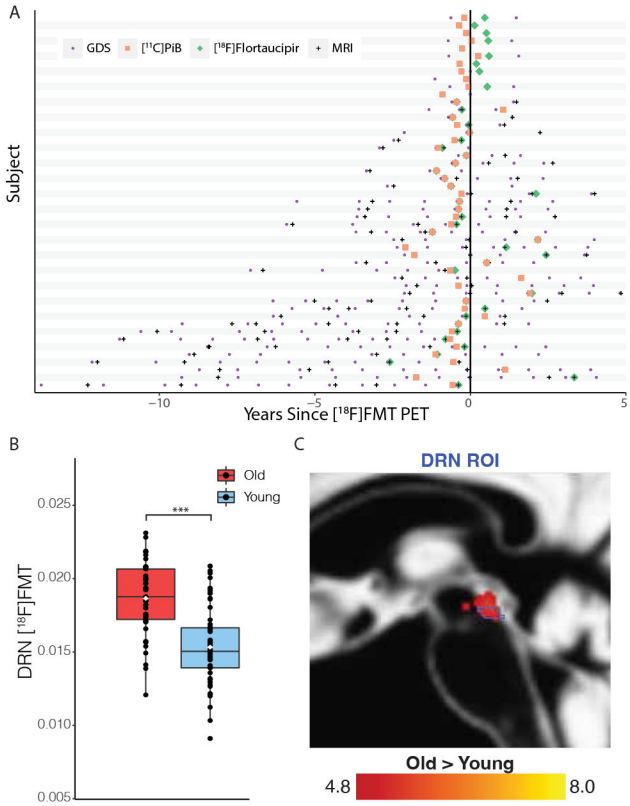

Figure 1: Timeline and Age-group differences in [^{18}F]FMT Ki:

(A) Timeline of older adult data (n = 49), including longitudinal MRI scans, longitudinal depression symptom testing sessions, [^{11}C]PiB PET, and [^{18}F]Flortaucipir PET relative to the [^{18}F]FMT PET scan shown at time 0 for each participant. (B) Tukey boxplot, with means shown as white diamonds. Older adults (red) show significantly higher [^{18}F]FMT Ki than younger adults (blue) in the dorsal raphe nucleus ($p < .001$***). (C) A whole-brain voxel-wise two-sample t-test comparing older adult [^{18}F]FMT Ki to young adult [^{18}F]FMT Ki showed regions of significantly higher [^{18}F]FMT Ki in older adults overlapping with the DRN (outlined in blue) region of interest (t-map overlay displayed at $p < 2.5 \times 10^{-6}$).

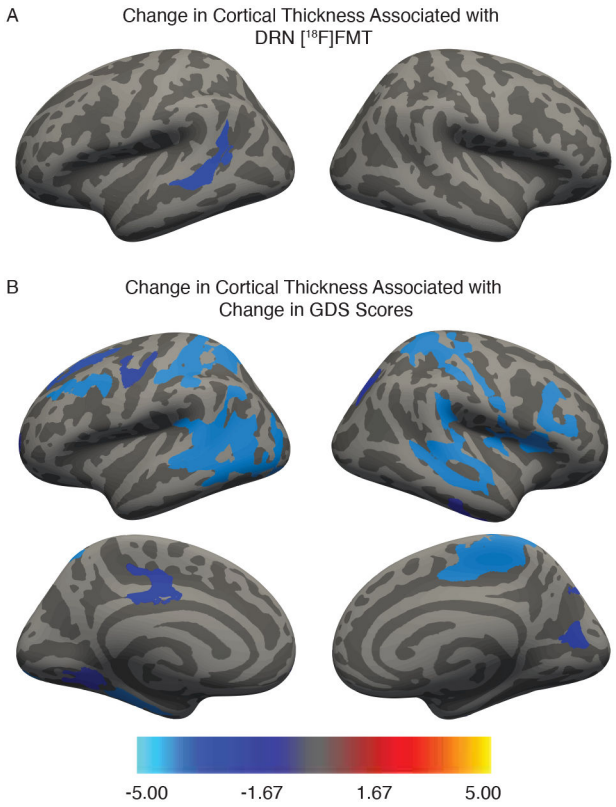

Figure 2: Relationships among cortical thickness changes, DRN [^{18}F]FMT, and depression symptom changes:

(A) Whole-brain vertex-wise regressions of dorsal raphe nucleus (DRN) [^{18}F]FMT Ki showed negative associations (cool colors) such that higher DRN [^{18}F]FMT Ki was associated with decreasing cortical thickness in the left temporal cortex. (B) Whole-brain vertexwise regression of depression symptom changes over time demonstrated that worsening depression symptoms were associated with decreasing cortical thickness. Color bars show significance using a −log(10) p-value scale. All analyses include Monte Carlo correction for multiple comparisons ($p < .05$).

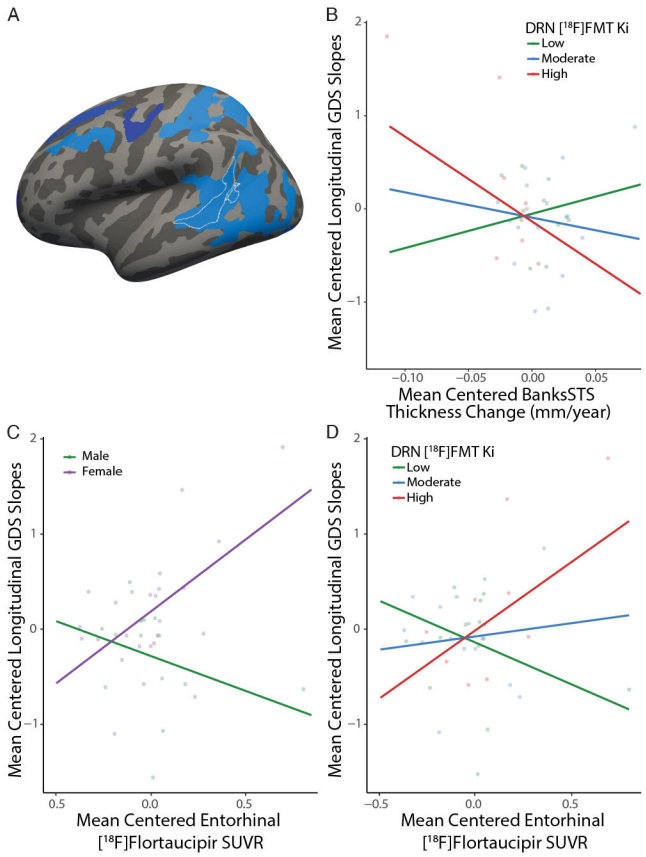

Figure 3: DRN [^{18}F]FMT Ki modulates relationships with depression symptom change: (A) Moderation analyses involving cortical thickness measured change in cortical thickness within the region outlined in white (left banks of the superior temporal sulcus, BanksSTS), which represents the region of overlap for both vertex-wise regression analyses displayed in Figure 2A,B. (B) Graphical representation of the conditional effects of dorsal raphe nucleus (DRN) [^{18}F]FMT Ki levels on atrophy and depression symptoms. Individuals with high levels of DRN [^{18}F]FMT Ki, defined as one standard deviation over the mean, show worsening depression symptoms with decreasing cortical thickness. (C) A significant sex by entorhinal cortex [^{18}F]Flortaucipir SUVR interaction predicting changes in depression symptoms, where females showed a significant positive relationship of higher tau burden and worsening depression symptoms over time. (D) Graphical representation of the moderating effects of DRN [^{18}F]FMT Ki on entorhinal cortex [^{18}F]Flortaucipir SUVR and depression symptoms. Individuals with high levels of DRN [^{18}F]FMT Ki show worsening depression symptoms with higher levels of entorhinal cortex [^{18}F]Flortaucipir SUVR.

Table 1:

Participant demographics, listed as the average ± standard deviation, for both young and old participants. Lower half of the table shows average [^{18}F]FMT Ki for different age groups, positive and negative [^{11}C]PiB status (no [^{11}C]PiB data for younger subjects), and males and females. GDS = Geriatric Depression Scale; FMT = Fluoro-m-tyrosine; MMSE = Mini Mental State Exam; DRN = dorsal raphe nucleus

	Older Adults	**Younger Adults**
Sample Size (N)	49	62
Age	77.10 ±5.98	22.08 ±3.25
Females/Males	29/20	35/27
Years of Education	16.61 ±2.04	
GDS (closest to [^{18}F]FMT PET)	3.82 ±3.23	
GDS Slopes (change/year)	0.04 ±0.70	
MMSE	28.71 ±1.17	
DRN [^{18}F]FMT Ki	0.0185 ±0.0024	0.0152 ±0.0025
[^{11}C]PiB Pos DRN [^{18}F]FMT Ki	0.0194 ±0.0023	
[^{11}C]PiB Neg DRN [^{18}F]FMT Ki	0.0181 ±0.0024	
Female DRN [^{18}F]FMT Ki	0.0191 ±0.0018	0.0150 ±0.0026
Male DRN [^{18}F]FMT Ki	0.0176 ±0.0029	0.0155 ±0.0025

Table 2:

(A) Results of the interaction analysis examining the effects of DRN [^{18}F]FMT Ki on the relationship between temporal lobe region cortical atrophy (mm/year) and Geriatric Depression Scale (GDS) scores over time ($p < .05$*). (B) Results of the interaction analysis examining the effects of DRN [^{18}F]FMT Ki on the relationship between entorhinal tau burden as measured with [^{18}F]Flortaucipir-PET and GDS scores over time ($p < .01$**).

	Variable	Estimate (B)	SE	95% CI	*β*	*t*	*p*
A	Cortical Atrophy	−2.21	4.22	−10.81, 6.40	−0.109	−0.522	0.605
	DRN [^{18}F]FMT Ki	−19.85	51.11	−123.97, 84.26	−0.068	−0.388	0.700
	Atrophy * [^{18}F]FMT	−3101.91	1507.61	−6172.82, −31.00	−0.428	−2.057	0.048*
B	DRN [^{18}F]FMT Ki	27.59	41.14	−55.93, 111.10	0.099	0.671	0.507
	[^{18}F]Flortaucipir SUVR	0.33	0.37	−0.42, 1.07	0.128	0.891	0.379
	[^{18}F]FMT * [^{18}F]Flortaucipir	501.64	155.40	186.16, 817.12	0.479	3.228	0.003**
	DV: GDS score change						